CANCER BIOTHERAPY AND RADIOPHARMACEUTICALS
Volume 38, Number 10, 2023
© Mary Ann Liebert, Inc.
DOI: 10.1089/cbr.2021.0389

Open camera or QR reader and scan code to access this article and other resources online.

Screening and Preclinical Evaluation of Novel Radiolabeled Anti-Fibroblast Activation Protein-α Recombinant Antibodies

Jianfeng Xu,[1,2] Shenghua Li,[3,4] Shasha Xu,[4] Juan Dai,[2] Zhigang Luo,[2] Jingjing Cui,[2] Fei Cai,[1,2] Changran Geng,[1] Zheng Wang,[2] and Xiaobin Tang[1]

Downloaded by Nanjing University of Chinese Medicine from www.liebertpub.com at 12/20/23. For personal use only.

Abstract

Background: Fibroblast activation protein-α (FAPα) is selectively overexpressed in tumor-associated fibroblasts in more than 90% of epithelial tumors, and may be a good target for anticancer treatment, for example, using an anti-FAPα recombinant antibody (rAb) labeled with radionuclides. In the present report, the radiolabeling and preclinical evaluation of novel anti-FAPα rAbs were investigated.

Materials and Methods: Two novel anti-FAPα VHHs (AMS002-1 and AMS002-2) with high binding affinity to FAPα were selected from an antibody phage library. The anti-FAPα VHHs were then fused with the Fc fragment of human IgG4 to create two VHH-Fc rAbs. The VHH-Fc rAbs were radiolabeled with ^{89}Zr and ^{177}Lu. The radiolabeled products were evaluated by radioligand-binding assays using FAPα-expressing cells. The biodistribution and tumor-targeting properties were investigated by small-animal PET/CT. AMS002-1-Fc, which showed promising tumor-targeting properties in ^{89}Zr-microPET imaging, was radiolabeled with ^{177}Lu for efficacy study on HT1080 tumor-bearing mice and monitored with SPECT/CT imaging.

Results: The two VHH-Fc rAbs with good affinity with K_D values in low nanomolar range were identified. Both PET/CT imaging with ^{89}Zr-AMS002-1-Fc rAb and SPECT/CT imaging with ^{177}Lu-AMS002-1-Fc rAb demonstrated highest tumor uptakes at 72 h p.i. and long tumor retention in the preclinical models. Furthermore, *ex vivo* biodistribution analysis revealed high tumor uptake of ^{89}Zr-AMS002-1-Fc at 48 h p.i. with the value of 6.91% ± 2.08% ID/g. Finally, radioimmunotherapy with ^{177}Lu-AMS002-1-Fc rAb delayed the tumor growth without significant weight loss in mice with HT1080 xenografts. The tumor size of untreated control group was 2.59 times larger compared with the treatment group with ^{177}Lu-AMS002-1-Fc at day 29.

Conclusion: ^{89}Zr/^{177}Lu-AMS002-1-Fc represent a pair of promising radiopharmaceuticals for theranostics on FAPα-expressing tumors.

Keywords: fibroblast activation protein-α, radiolabeled nanobody, radiotherapy, VHH-Fc, theranostics

[1]Department of Nuclear Sciences and Technology, Nanjing University of Aeronautics and Astronautics, Nanjing, People's Republic of China.
[2]JYAMS PET Research and Development Limited, Nanjing, People's Republic of China.
[3]College of Life Sciences & Health, Wuhan University of Science and Technology, Wuhan, People's Republic of China.
[4]Beijing Novabody Biotechnological Ltd., Beijing, People's Republic of China.

Address correspondence to: Zheng Wang; JYAMS PET Research and Development Limited; No. 568 Longmian Avenue, Nanjing 211100, People's Republic of China
E-mail: **wangzheng@amschina.com**

Xiaobin Tang; Department of Nuclear Sciences and Technology, Nanjing University of Aeronautics and Astronautics; No. 29 Jiangjun Avenue, Nanjing 211016, People's Republic of China
E-mail: **tangxiaobin@nuaa.edu.cn**

Downloaded by Nanjing University of Chinese Medicine from www.liebertpub.com at 12/20/23. For personal use only.

Introduction

The tumor microenvironment (TME) is the complex environment in which various noncancerous stromal cell populations coexist, coevolve, and interact with tumor cells, possessing a profound impact on the progression of solid tumors. Cancer-associated fibroblasts (CAFs) are an essential component of the TME and play a key role in tumorigenesis, neoplastic progression, angiogenesis, invasion, and metastasis of a tumor. Fibroblast activation protein-α (FAPα) is an important surface marker of CAFs.

FAPα, which is a cell surface-bound type II transmembrane glycoprotein, belongs to the member of the serine protease family and is expressed in the microenvironment of more than 90% of epithelial tumors, including pancreas, colon, breast, and carcinomas.[1] FAPα expression in healthy tissue is relatively low.[2] FAPα is expressed on CAFs within the tumor stroma, which is a major part of a tumor's composition.[3] While in most tumor types FAPα was predominantly localized to the stroma, FAP expression was also observed in tumor cells, especially in tumors of mesenchymal origin, for example, sarcoma and mesothelioma.[4,5]

FAPα has become a potential antitumor target due to the characteristic of overexpression in CAFs rather than normal tissues and the close relation to tumorigenesis, invasion, metastasis, and immunosuppression. Meta-analysis indicates that patients with FAPα overexpression have a higher risk of tumor invasion, lymph node metastasis, and worse prognosis.[6] Thus, FAPα has emerged as the next pan-cancer target for diagnostic and therapeutic development.

At present, a variety of methods for targeting FAPα have been developed using antibodies,[7–10] peptide prodrugs,[5,11] or small molecules.[12–14] First-generation FAP inhibitors (FAPIs) have shown good affinity but plagued by a lack of selectivity with respect to related enzymes. Second-generation quinoline-based FAPIs are coupled to a 2-cyanopyrrolidine moiety and have been demonstrated nanomolar affinity and high specificity for FAP with interfering dipeptidyl peptidases.[15,16] When radiolabeled, ^{68}Ga-FAPI-04/FAPI-46 showed excellent imaging properties that applied for a variety of clinical cancer indications.

However, FAPIs are still limited by their relatively short tumor retention time. FAP-2286 peptide increased the circulating life and exhibited excellence in clinical trial, but the effective half-life of ^{177}Lu-FAP-2286 in the whole body (35 h) was still a concern for reporters.[5]

Furthermore, modified FAP-specific antibodies have recently gained interest. A first-generation anti-FAPα antibody F19 (sibrotuzumab) displayed excellent tumor stroma-targeting properties but failed to show measurable therapeutic activity in phase I/II clinical trials.[17,18] Moreover, two new anti-FAPα antibodies ESC11 and ESC14, which are labeled with ^{177}Lu, have shown excellent targeting in melanoma xenografts.[4,19] However, the large molecular size of the intact antibodies prevents the deep tumor penetration and leads to slow systemic clearance, eventually leading to low-contrast images.[20,21]

Single-domain antibodies (sdAbs, VHHs, or Nanobodies) are featured by their small size, and show high specificity and affinity to many different types of antigens and a lower off-target accumulation.[22] Furthermore, nanobodies have the inherent favorable features of penetrating dense tissues like tumors.[23] Numerous nanobodies have already been demonstrated useful for basic and advanced research in therapy and diagnostics of cancer.[24] However, targeting of FAPα with radiolabeled nanobodies is rarely investigated. Therefore, we hypothesized that radioimmunoimaging and radioimmunotherapy with anti-FAPα nanobodies might be an attractive noninvasive diagnostic and therapeutic tool in FAPα-positive tumor(s).

In the present study, two VHHs were selected by surface plasmon resonance technology (SPR) and fused with a human IgG4 Fc to form two anti-FAPα recombinant antibodies (rAbs). The two rAbs were labeled with ^{89}Zr/^{177}Lu for PET/CT and SPECT/CT imaging studies, respectively. The efficacy study of ^{177}Lu-AMS002-1-Fc was conducted on FAPα-expressing tumor xenografts and showed effective radiotherapy result.

Materials and Methods

Preparation and characterization of anti-FAPα rAb

Alpacas were immunized subcutaneously for six times at an interval of 14–21 d with total amount of 2 mg recombinant human FAPα protein obtained from Sino Biological, Inc. (Beijing, China). After titration of the antiserum, 70 mL of blood was collected, and the peripheral blood mononuclear cells were isolated. Total RNA was extracted, and VHH genes ($\sim$500 bp) were cloned into the phagemid and transformed into *Escherichia coli* TG1 cells. The amplified and purified phage were enriched and screened on antigen-coated immunotubes by solid-phase screening method for three rounds to obtain optimized FAPα VHHs AMS002-1 and AMS002-2 with high specificity and affinity. The binding capacity to FAPα was verified by ELISA assay. All animal studies were performed in accordance with the protocols provided in the Guide for the Care and Use of Medical Laboratory Animals (Ministry of Health, China).

FAPα-Fc fusion proteins were obtained from gene synthesis, which are referred to as AMS002-1-Fc and AMS002-2-Fc. This Fc was chosen from amino acid fragment from *E219* to *K449* of Human IgG4, with two amino acid mutations at *S229P/R409K* for Fc dimerization stability. The fusion protein was expressed in HEK293 cells and purified by Protein A affinity chromatography column. Sodium dodecyl sulfate–polyacrylamide gel electrophoresis (SDS-PAGE) and SEC high-performance liquid chromatography (HPLC) were performed for quality control.

The Biosensor instrument (Biacore T200; GE Healthcare) was used to measure the equilibrium dissociation constant (K_D) using SPR by human IgG (Fc) capture method. Sensorgrams were shown in Figure 1, Supplementary Figures S3 and S4.

Chelator conjugation and radiolabeling

For ^{89}Zr radiolabeling, *p*-NCS-Bz-DFO was used. In brief, 8–10 mg of VHH-Fc rAbs was incubated with 10 equivalents of *p*-NCS-Bz-DFO in Na_2CO_3 buffer (pH 9.0) at 37°C for 1 h, and then purified on a PD-10-size exclusion chromatography column using sodium acetate buffer (pH 7.0) as mobile phase. The *p*-NCS-Bz-DFO-conjugated VHH-Fc rAbs were subsequently radiolabeled with ^{89}Zr using the previously reported method.[25] Around 370 MBq of ^{89}Zr-oxalate solution in 1.0 M oxalic acid ($\sim$500 μL) was neutralized with Na_2CO_3 solution at pH 7.0 and then mixed

with 5 mg of DFO-rAb and 1.0 mL of sodium acetate buffer, followed by incubation for 60 min at room temperature. The reaction mixture was purified by PD-10 columns using 0.9% saline as mobile phase to obtain ^{89}Zr-labeled VHH-Fc rAb.

For ^{177}Lu labeling, *p*-NCS-Bn-DOTA was used. VHH-Fc rAbs were conjugated with *p*-NCS-Bn-DOTA with a reactant molar ratio of 1:10 incubated in Na_2CO_3 buffer (pH 9.0) at 37°C for 1 h. The conjugate was purified on a PD-10 column using sodium acetate buffer (pH 5.5) as mobile phase. The *p*-NCS-Bn-DOTA-conjugated VHH-Fc rAbs were subsequently radiolabeled with ^{177}Lu using the previously reported method.[26–28] $^{177}LuCl_3$ (370 MBq) was diluted in 300 μL of sodium acetate buffer and then added to 5 mg of DOTA-rAb. The reaction mixture was incubated for 60 min at 37°C with constant shaking. ^{177}Lu-labeled VHH-Fc rAb was then purified by PD-10 column using 0.9% saline as mobile phase.

The chelator-to-antibody ratio (DAR) was determined by liquid chromatography–mass spectrometry (LC-MS).

Radiochemical purity

The final product was assessed by instant thin-layer chromatography (iTLC), as well as a HPLC system (1260 Infinity; Agilent Technologies) fitted with a B-FC-3300 detector and a TSK Gel G2000SWXL column for radiolabeling efficiency and radiochemical purity. As the mobile phases, 0.5 M of citric acid solution was used for iTLC and mixture of 0.1 M PBS and 0.2 M NaCl in 10% acetonitrile solution was used at a flow rate of 0.8 mL/min for HPLC.

Cell lines and animal models

The two cell lines with different expression levels of FAPα were selected, human fibrosarcoma HT1080 cell line and human non-small cell lung cancer A549 cell line, respectively. HT1080 cell line was purchased from Hunan Fenghui Biotechnology Co., Ltd (Changsha, China). A549 cell line was purchased from Nanjing Cobioer Biosciences Co., Ltd (Nanjing, China). BALB/c mice bearing HT1080 or A549 xenografts were obtained from Jiangsu Keygen Biotech Corp. Ltd (Nanjing, China). All animal studies were performed in accordance with the protocols provided in the Guide for the Care and Use of Medical Laboratory Animals (Ministry of Health, China). An equal number of males and females were used for each cohort.

Micro-PET/CT imaging

Micro-PET/CT experiments were conducted using mice bearing HT1080 xenografts and A549 xenografts. The mice were administered intravenously with ~3.7 MBq (100 μg) of AMS002-1-Fc or AMS002-2-Fc labeled with ^{89}Zr ($n = 3$–4 per group) through the tail vein. A whole-body scan was performed on mice at 24, 48, 72, and 216 h after injection. At each time point, the acquisition time was 10–30 min at 350–650 keV of photopeak window using a preclinical *in vivo* imaging equipment (SNPC-103; Pingseng Healthcare, Inc.). At each time point, the mice were positioned in the scanner after anesthetizing with isoflurane. CT scans were conducted before or after PET scans.

The images were reconstructed and decay corrected using the PMOD Biomedical Image Quantification System (PMOD) software. The region of interests (ROI) was manually drawn around tumor and within muscle tissue (as background). For quantification of radiotracer accumulation in the tumors (%ID/g), the target/background ratios were calculated. Noncompartmental model was adopted to calculate pharmacokinetic parameters of VHH-Fc rAbs in various tissues using drug and statistics software version 3.2.8.

Ex vivo *biodistribution*

The mice were injected with 3.7 MBq (100 μg) of ^{89}Zr-AMS002-1-Fc or ^{89}Zr-AMS002-2-Fc and euthanized at the 48 and 216 h p.i. time point, respectively. Blood was withdrawn from the heart for approximately 0.2–0.5 mL, and the selected organs/tissue were collected, including heart, liver, spleen, lungs, kidneys, pancreas, stomach, small intestine, large intestine, muscle, brain, tibia, arthrosis, and tumor. The collected organs/tissues were weighed and counted using an automated gamma counter (GC-1200; Anhui Ustc Zonkia Scientific Instruments CO., LTD).

Cell uptake, internalization, and efflux studies

For cell uptake studies, HT1080 cells and A549 cells were seeded in poly (L-lysine)-coated 24-well cell culture plates, respectively, at a density of 2×10^5 cells per well and incubated with 37 kBq (1 μCi)/well of ^{89}Zr-AMS002-1-Fc at 37°C for 4, 24, and 72 h. After incubation, the cells were washed twice with 0.5 mL cold PBS to collect supernatants and lysed with 0.5 mL digestion (1 M) to collect cell precipitation. Internalization assay was preformed similarly to the procedure described above. After 4, 24, and 72 h incubation of HT1080 cells and A549 cells with ^{89}Zr-AMS002-1-Fc at 37°C, the cells were washed twice with cold PBS and then incubated with 0.5 mL of glycine–HCl in PBS (50 mM, pH 2.8) for 2 min at room temperature.

Thereafter, the cells were washed twice with 0.5 mL cold PBS to collect supernatants and lysed with 0.5 mL digestion (1 M) to collect cell precipitation. For efflux experiment, the cells were then washed twice with cold PBS, and incubated with complete medium at 37°C for 24 h. At each time point, the cells were washed twice with 0.5 mL cold PBS to collect supernatants and lysed with 0.5 mL digestion (1 M) to collect cell precipitation. The supernatants and cell lysates were collected and measured in a gamma counter. Each data point is an average of four wells.

Immunohistochemistry

The xenografted tumor FAPα expression levels were confirmed by using immunohistochemistry. BALB/c mice bearing HT1080 or A549 xenografts were euthanized. Tumor tissues were collected and fixed with 4% paraformaldehyde. After dehydration, the tissue was embedded in paraffin, snap frozen, and sliced into 5 μm sections. The slices were rinsed with PBS three times after dewaxing and rehydrating, and then blocked with 5% BSA in the dark at room temperature for 1 h. The slices with 1:50 FITC-labeled anti-FAPα antibodies were incubated in the dark at 4°C overnight for FAPα staining. Next, the slices were stained with Hoechst for 15 min. Finally, fluorescence images were acquired with 630 × magnification at 1024 × 1024 pixel resolution using the laser confocal microscope (LSM 710; Carl Zeiss).

Downloaded by Nanjing University of Chinese Medicine from www.liebertpub.com at 12/20/23. For personal use only.

Downloaded by Nanjing University of Chinese Medicine from www.liebertpub.com at 12/20/23. For personal use only.

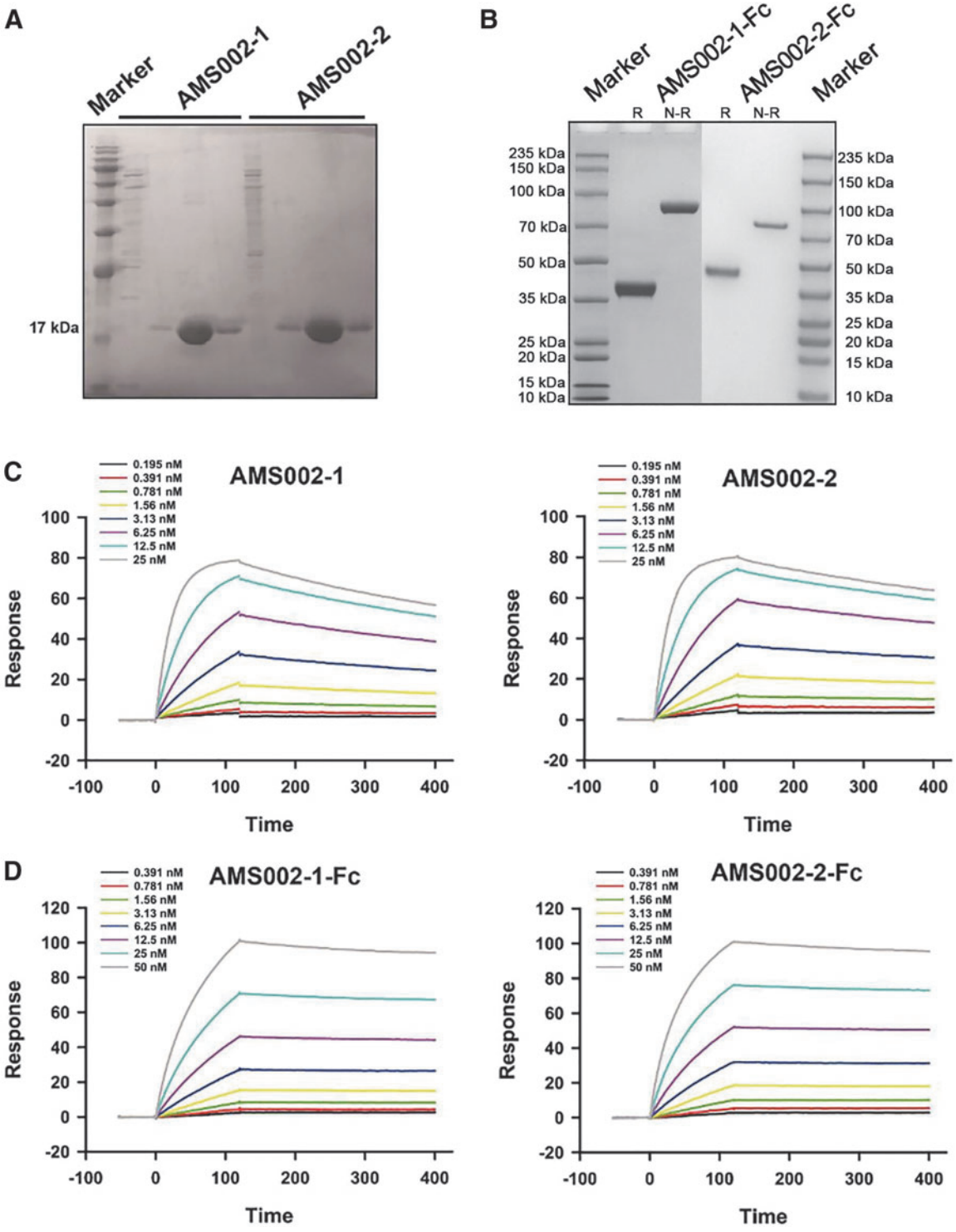

FIG. 1. Characterization and specificity of anti-FAPα VHHs and VHH-Fc rAbs. **(A)** SDS-PAGE analysis of purified VHHs, as compared with a ladder ranging from 200 to 10 kDa. **(B)** SDS-PAGE analysis of purified VHH-Fc rAbs under reducing or nonreducing conditions, as compared with a ladder ranging from 235 to 10 kDa. **(C, D)** Affinity of AMS002-1, AMS002-2, AMS002-1-Fc, and AMS002-2-Fc was determined by SPR. SPR, surface plasmon resonance; SDS-PAGE, sodium dodecyl sulfate–polyacrylamide gel electrophoresis.

Downloaded by Nanjing University of Chinese Medicine from www.liebertpub.com at 12/20/23. For personal use only.

Pharmacokinetic studies in rats

Around 3.7 MBq (100 μg) of ^{89}Zr-AMS002-1-Fc was injected intravenously into 3 female and 3 male SD rats ($n=6$). At different predetermined intervals, 0.1–0.2 mL of jugular bulb blood was drawn at 5 min, 2, 8, 12, 24, 48, 72, 96, 120, 168, 216, and 336 h. Radioactivity for collected blood samples was counted for 30 s by using the gamma counter (GC-1200; Anhui Ustc Zonkia Scientific Instruments CO., LTD).

Micro-SPECT/CT imaging

Micro-SPECT/CT experiments were performed using a dedicated small-animal SPECT/CT camera (NanoScan; Mediso Medical Imaging Systems). The SPECT/CT scans were acquired at 24, 72, 120, and 240 h p.i. with time deviation controlled within ±5%. At each time point, the mice were positioned in the scanner after anesthetizing with isoflurane and scanned for 10–30 min. CT scans were conducted before or after SPECT scans. The images were reconstructed and decay corrected using the PMOD software. The ROI was manually drawn around tumor and within muscle tissue.

Radiotherapy studies

For a proof-of-concept study, only AMS002-1-Fc was used. Therapy study was conducted using human fibrosarcoma HT1080 tumor-bearing mice, which were injected with saline (the control group, $n=8$), $^{177}LuCl_3$ (the control group, 14.8 MBq, $n=8$), or ^{177}Lu-AMS002-1-Fc (14.8 MBq, about 140 μg, $n=12$). Tumor size and animal body weight were measured every day from the date of injection (day 0) until completion of the study (day 29). Endpoint criteria were defined as a tumor volume exceeding 4000 mm^3 or critical scoring of an animal's wellbeing. With limited amount of rAb produced, the saline and $^{177}LuCl_3$ were used as the controls.

Statistical analysis

Quantitative data are expressed as mean ± standard deviation (SD). Mean between different groups were compared using Student's *t*-test, and $p<0.05$ indicates statistical significance ($^*p<0.05$, $^{**}p<0.01$, and $^{***}p<0.001$).

Results

Characterization and specificity of anti-FAPα rAbs

SDS-PAGE gel of purified VHHs and VHH-Fc rAbs showed a characteristic band under reducing conditions (Fig. 1A, B). The molecular weight of VHH was 17 kDa and VHH-Fc rAb was close to the theoretical value of 38 kDa. The electrophoretic purity was more than 95%. The VHH-Fc rAb existed as a dimeric form so that the molecular weight of AMS002-1-Fc and AMS002-2-Fc was 76 kDa. The amino acid sequence was also detected (Supplementary Table S1).

The binding affinity to recombinant huFAP was determined by SPR measurement using chips coated with a low density of huFAP (Fig. 1C, D). The results showed K_D values of 0.654 nM for VHHs AMS002-1 and 0.393 nM for AMS002-2, respectively (Table 1). K_D values of 0.547 and 0.307 nM were calculated for VHH-Fc rAbs AMS002-1-Fc and AMS002-2-Fc, respectively (Table 1). Conjugation and chelation had little effect on antibody affinity (Supplementary Fig. S3).

The average DAR value of DFO-AMS002-1-Fc was 1.7 (DAR0: 8.6%, DAR1: 29.9%, DAR2: 42.3%, DAR3: 17.0%, DAR4: 2.2%). The average DAR value of DOTA-AMS002-1-Fc was 1.6 (DAR0: 4.3%, DAR1: 44.2%, DAR2: 41.2%, DAR3: 7.3%, DAR4: 2.9%) as demonstrated in Supplementary Figure S6.

High radiochemical yields were observed, with 63% for ^{89}Zr-AMS002-1-Fc, 65% for ^{89}Zr-AMS002-2-Fc, and 68% for ^{177}Lu-AMS002-1-Fc, respectively. The radiochemical purity of the final products was greater than 95% (Supplementary Fig. S1). The specific activity of ^{89}Zr-AMS002-1-Fc and ^{89}Zr-AMS002-2-Fc was 37 MBq/mg, and that of ^{177}Lu-AMS002-1-Fc was 106 MBq/mg. The *in vitro* stability was shown in Supplementary Figure S2.

Micro-PET/CT imaging, in vivo *biodistribution and* ex vivo *biodistribution*

The whole-body PET/CT images of mice bearing FAPα-positive xenografts from 24 to 216 h after injection of radiotracer are shown in Figure 2. The results showed that the radiotracer had a lower distribution in the brain and muscle and showed a progressive reduction through the observed period. Spleen is an immune organ capable of partial immune uptake of antibodies. Liver and kidneys are organs

Table 1. Affinity Kinetics Determined by Surface Plasmon Resonance

Method	*Ligand*	*Analyte*	k_a *(1/Ms)*	k_d *(1/s)*	K_D *(nM)*
Human IgG (Fc) Capture	FAP-Fc	AMS002-1	1.82×10^{6}	1.19×10^{-3}	0.654
Human IgG (Fc) Capture	FAP-Fc	AMS002-2	1.99×10^{6}	7.83×10^{-4}	0.393
Human IgG (Fc) Capture	AMS002-1-Fc	FAP-His	3.55×10^{5}	1.94×10^{-4}	0.547
Human IgG (Fc) Capture	AMS002-2-Fc	FAP-His	4.62×10^{5}	1.42×10^{-4}	0.307
Human IgG (Fc) Capture	DFO-AMS002-1-Fc	Human FAP	2.90×10^{5}	1.61×10^{-4}	0.556
Human IgG (Fc) Capture	DOTA-AMS002-1-Fc	Human FAP	2.75×10^{5}	5.78×10^{-5}	0.211
Human IgG (Fc) Capture	^{91}Zr-DFO-AMS002-1-Fc	Human FAP	2.77×10^{5}	1.45×10^{-4}	0.524
Human IgG (Fc) Capture	^{175}Lu-DOTA-AMS002-1-Fc	Human FAP	2.93×10^{5}	1.26×10^{-4}	0.428
Human IgG (Fc) Capture	AMS002-1-Fc	Cynomolgus FAP	2.66×10^{5}	1.20×10^{-4}	0.450
Human IgG (Fc) Capture	AMS002-2-Fc	Cynomolgus FAP	3.71×10^{5}	5.48×10^{-5}	0.148
Human IgG (Fc) Capture	AMS002-1-Fc	Mouse FAP		No binding	
Human IgG (Fc) Capture	AMS002-2-Fc	Mouse FAP		No binding	

Equilibrium dissociation constant (K_D), association constant (k_a), and dissociation constant (k_d) of the different VHHs and VHH-Fc rAbs binding to FAP by human IgG (Fc) capture method.

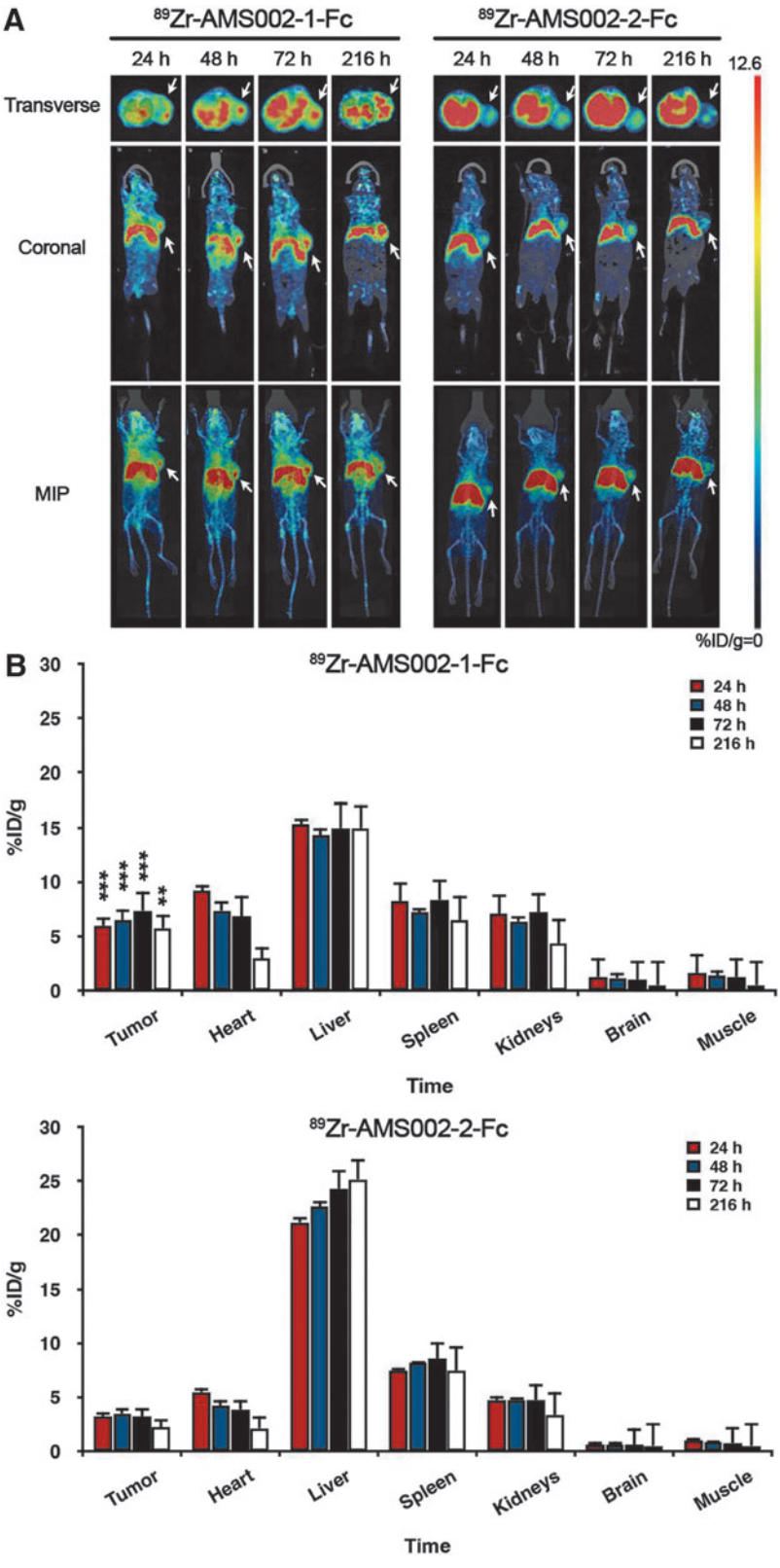

FIG. 2. Analysis of ^{89}Zr-AMS002-1-Fc- and ^{89}Zr-AMS002-2-Fc-treated HT1080 tumor xenografts **(A)** Whole-body micro-PET/CT imaging of BALB/c nude mice bearing HT1080 xenografts (*white arrows*) after injection of 3.7 MBq (100 μg) of ^{89}Zr-AMS002-1-Fc and ^{89}Zr-AMS002-2-Fc. **(B)** Quantitative analysis of ROIs of BALB/c nude mice bearing HT1080 xenografts after injection of 3.7 MBq (100 μg) of ^{89}Zr-AMS002-1-Fc and ^{89}Zr-AMS002-2-Fc. Each data point represents mean ± SD ($n = 3$–4). $^{**}p < 0.01$ and $^{***}p < 0.001$. ROI, region of interests.

related to metabolism with high uptake value. The liver uptake of ^{89}Zr-AMS002-1-Fc was about 15% ID/g and that of ^{89}Zr-AMS002-2-Fc increased from 21.19% ± 0.70% ID/g (24 h p.i.) to 25.19% ± 1.49% ID/g (216 h p.i.). The renal uptake of ^{89}Zr-AMS002-1-Fc decreased from 7.12% ± 1.66% ID/g (24 h p.i.) to 4.37% ± 1.08% ID/g (216 h p.i.), and that of ^{89}Zr-AMS002-2-Fc decreased from 4.79% ± 0.85% ID/g (24 h p.i.) to 3.33% ± 0.63% ID/g (216 h p.i.).

The tumor uptake of ^{89}Zr-AMS002-1-Fc peaked at 72 h p.i. with 7.37% ± 0.54% ID/g and also had a good retention

Downloaded by Nanjing University of Chinese Medicine from www.liebertpub.com at 12/20/23. For personal use only.

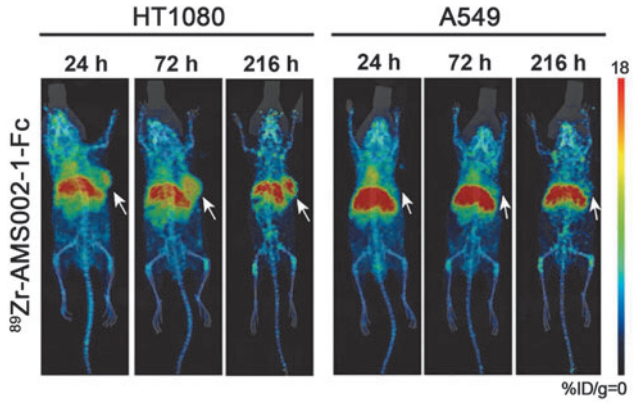

FIG. 3. Whole-body micro-PET/CT imaging of ^{89}Zr-AMS002-1-Fc (3.7 MBq, 100 μg) on BALB/c nude mice bearing HT1080 and A549 xenografts (*white arrows*). MIPs of representative mice were shown at three different time points after injection ($n = 3$ per group). MIP, maximum intensity projection.

at 216 h p.i. (5.69% ± 1.71% ID/g). In marked contrast, the uptake value of ^{89}Zr-AMS002-2-Fc in tumor lesion was between 2% and 3% ID/g with no significant change during the study period. Although uptake value was high in the heart, it decreased rapidly after injection (Fig. 2B).

The *in vivo* biodistribution of ^{89}Zr-AMS002-1-Fc was further studied over time in mice bearing A549 xenografts (Fig. 3). Compared with FAPα-expressing HT1080 cells, ^{89}Zr-AMS002-1-Fc had much less accumulation in A549 tumor than that in HT1080 cells at all the time points, indicating its selective targeting specificity in different types of tumors. This is consistent with the results of *in vitro* cell uptake (Fig. 4) and *ex vivo* immunofluorescence (Supplementary Fig. S5).

The *ex vivo* biodistribution of ^{89}Zr-AMS002-1-Fc and ^{89}Zr-AMS002-2-Fc in BALB/c nude mice bearing HT1080 xenografts at 48 and 216 h postinjection is shown in Table 2. The radioactivity of ^{89}Zr-AMS002-1-Fc in tumor was more than 6% ID/g over time. However, tumor uptake of ^{89}Zr-AMS002-2-Fc decreased from 5.24% ± 0.77% ID/g (48 h p.i.) to 1.69% ± 0.23% ID/g (216 h p.i.).

The high uptake of liver and kidneys may be due to the physicochemical properties of nanobodies, which are metabolized and/or eliminated by the liver and kidneys. Hepatic metabolism is increased with high liver uptake at a late time point. The renal metabolism is gradually cleared with a lower renal uptake at a late time point. However, spleen is an immune organ capable of partial immune uptake of antibodies with high uptake value all the time. There was extreme low uptake of the radiotracer found in muscle and brain tissues.

The tumor-to-muscle and tumor-to-blood ratios of ^{89}Zr-AMS002-1-Fc were much higher compared with ^{89}Zr-AMS002-2-Fc at 48 and 216 h p.i. ^{89}Zr-AMS002-1-Fc displayed the highest tumor-to-muscle ratio of 13.18 ± 6.63 and a tumor-to-blood ratio of 3.57 ± 1.10 at 216 h p.i. In contrast, the tumor-to-muscle ratio and tumor-to-blood ratio of ^{89}Zr-AMS002-2-Fc at 216 h p.i. were 2.51 ± 0.61 and 0.89 ± 0.18, respectively.

Cell uptake, internalization, and efflux studies

^{89}Zr-AMS002-1-Fc showed much higher cell uptakes in the HT1080 cells than in the A549 cells at 4, 24, and 72 h of incubation. ^{89}Zr-AMS002-1-Fc internalized in the HT1080 cells faster than in the A549 cells. Within the first 4 h of incubation, the efflux rate in the HT1080 cells was similar to that in the A549 cells. The efflux rate in the HT1080 cells became faster at 24 h and later time points (Fig. 4).

Histological analysis of AMS002-1-Fc on the FAPα-expressing tumors

To further examine the expression of FAPα in human tumor tissues, the immunohistochemical staining of AMS002-1-Fc on tissue slices from HT1080 and A549 xenografts were evaluated. Representative immunohistochemistry staining revealed that FAPα fluorescence signals bound to HT1080 and A549 in various degrees (Fig. 5).

Pharmacokinetics studies

^{89}Zr-AMS002-1-Fc displayed blood clearance over the 14-d time course, with 4.87% ± 1.24% ID/g at 5 min and 0.80% ± 0.23% ID/g at 120 h postinjection. The blood half-life of ^{89}Zr-AMS002-1-Fc is 128 h (Fig. 6).

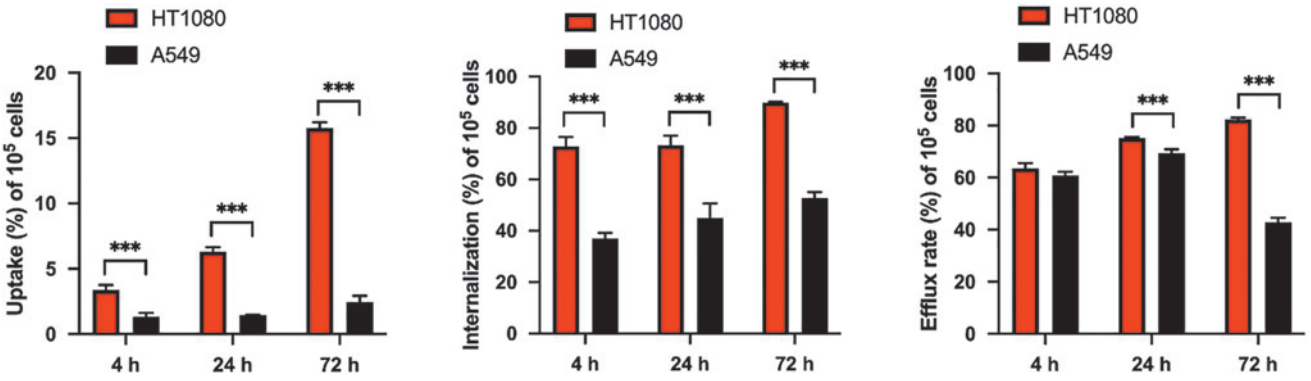

FIG. 4. Cell uptake, internalization, and efflux studies of ^{89}Zr-AMS002-1-Fc in HT1080 and A549 tumor cells. Data are presented as mean ± SD. ***$p < 0.001$.

Downloaded by Nanjing University of Chinese Medicine from www.liebertpub.com at 12/20/23. For personal use only.

TABLE 2. *EX VIVO* BIODISTRIBUTION OF ^{89}ZR-AMS002-1-FC AND ^{89}ZR-AMS002-2-FC IN BALB/C NUDE MICE BEARING HT1080 XENOGRAFTS

	^{89}Zr-AMS002-1-Fc		*^{89}Zr-AMS002-2-Fc*	
Organs and tissues	*48 h*	*216 h*	*48 h*	*216 h*
Heart	2.70 ± 0.75	1.74 ± 0.26	4.25 ± 0.75	1.96 ± 0.49
Liver	14.69 ± 3.45	18.63 ± 1.43	7.08 ± 0.41	20.48 ± 3.63
Spleen	9.37 ± 2.74	26.86 ± 4.85	19.34 ± 5.53	15.38 ± 1.93
Lungs	6.07 ± 1.17	4.51 ± 0.22	6.81 ± 0.84	2.57 ± 0.39
Kidneys	11.69 ± 1.92	8.61 ± 3.73	9.24 ± 2.57	3.87 ± 0.91
Pancreas	2.42 ± 0.74	1.91 ± 0.81	2.49 ± 0.58	1.30 ± 0.80
Stomach	1.73 ± 0.50	1.27 ± 0.05	1.77 ± 0.31	0.71 ± 0.23
Small intestine	1.64 ± 0.19	0.83 ± 0.17	1.57 ± 0.31	0.44 ± 0.04
Large intestine	1.66 ± 0.40	0.93 ± 0.12	1.39 ± 0.45	0.46 ± 0.08
Muscle	0.90 ± 0.18	0.50 ± 0.08	1.57 ± 0.42	0.71 ± 0.25
Brain	0.38 ± 0.06	0.28 ± 0.07	0.43 ± 0.12	0.18 ± 0.04
Tibia	5.01 ± 2.13	6.97 ± 2.80	5.56 ± 2.53	3.52 ± 1.86
Arthrosis	4.95 ± 1.33	7.00 ± 2.84	3.37 ± 0.55	3.05 ± 0.50
Tumor	6.91 ± 2.08	6.20 ± 2.01	5.24 ± 0.77	1.69 ± 0.23
Tumor/Blood	2.87 ± 1.73	3.57 ± 1.10	1.24 ± 0.07	0.89 ± 0.18
Tumor/Muscle	7.73 ± 1.69	13.18 ± 6.63	3.43 ± 0.48	2.51 ± 0.61

Each data point represents mean ± SD (n = 3–4).

Micro-SPECT/CT imaging in mice bearing HT1080 xenografts

Figure 7 gives micro-SPECT/CT images and semiquantitative analysis of ROIs of tumor-bearing mice administered with 14.8 MBq (140 μg) of ^{177}Lu-AMS002-1-Fc. The results showed that the tumor uptake peaked 5.96% ± 0.64% ID/g at 72 h p.i. and maintained 2.85% ± 1.17% ID/g at 240 h p.i. (Fig. 7B). The liver uptake decreased over time from 7.65% ± 0.89% ID/g (24 h p.i.) to 5.55% ± 1.89% ID/g (240 h p.i.). The kidney uptake was slightly higher than the tumor uptake at all the time points. The tibia uptake was low with 0.67% ± 0.87% ID/g at 24 h p.i. and declined over time. The muscle uptake was nearly none through the observed period.

Therapeutic efficacy of ^{177}Lu-AMS002-1-Fc-treated HT1080 tumor xenografts

Figure 8 demonstrates tumor growth curves of ^{177}Lu-AMS002-1-Fc as well as negative controls, saline, and $^{177}LuCl_3$, in mice bearing HT1080 xenografts. The therapeutic efficacy of a single dose of the ^{177}Lu-AMS002-1-Fc *in vivo* was investigated. There were no significant discrepancies in the volumes of HT1080 tumors for all groups before therapy. After therapy, the average tumor volume of ^{177}Lu-AMS002-1-Fc group was always smaller than 1500 mm^3 (1093.16 ± 382.49 mm^3 at day 29), whereas that of the untreated control group was increasing gradually and eventually reaching up to 2829.02 ± 1165.54 mm^3 at day 29

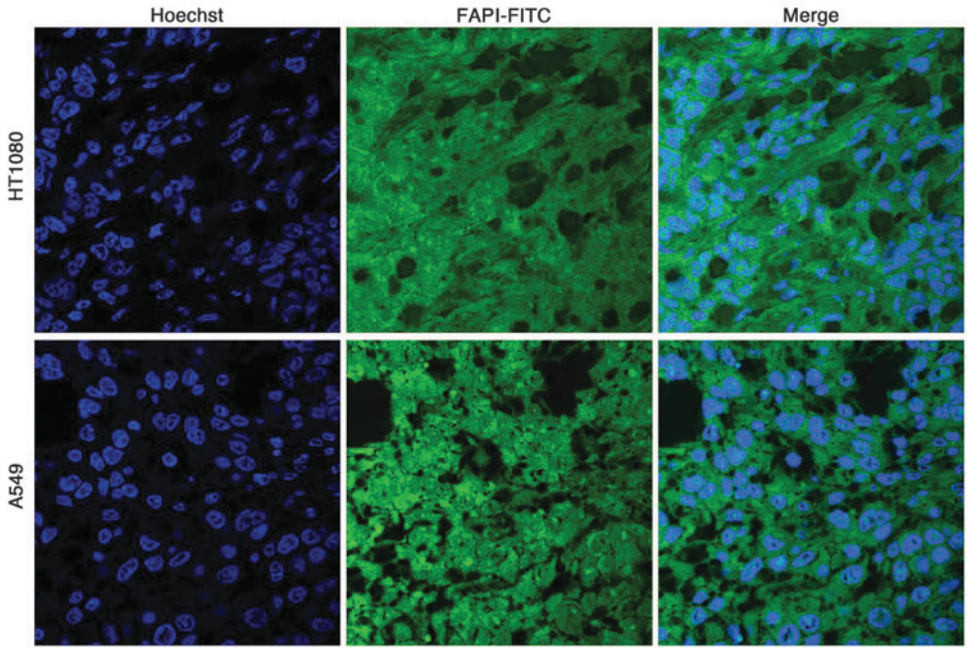

FIG. 5. Representative confocal microscopy images of tumor in the mice bearing HT1080 and A549 xenografts incubated with AMS002-1-Fc at 630× magnification.

Downloaded by Nanjing University of Chinese Medicine from www.liebertpub.com at 12/20/23. For personal use only.

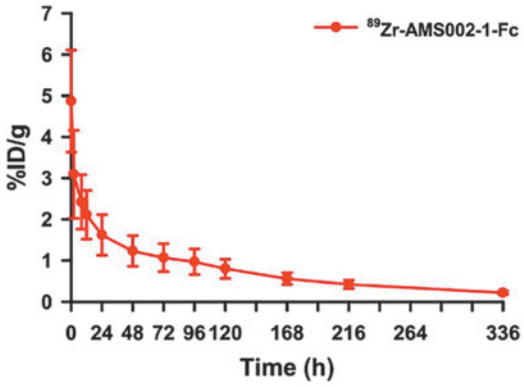

Parameter	Unit	Value
$t_{1/2}$	h	128.06 ± 25.70
T_{max}	h	0.08 ± 0.00
C_{max}	%ID/g	4.87 ± 1.24
C_0	%ID/g	4.97 ± 1.30
AUC_{0-t}	(%ID/g)*h	258.36 ± 68.93
AUC_{0-inf}	(%ID/g)*h	298.64 ± 69.23
MRT_{0-inf}	h	163.38 ± 28.70

FIG. 6. Pharmacokinetics study of ^{89}Zr-AMS002-1-Fc. Blood kinetics of ^{89}Zr-AMS002-1-Fc after a single intravenous administration. Each data point represents mean ± SD ($n = 3$).

(Fig. 8A). The tumor size of untreated control group was 2.59 times larger compared with the treatment group with ^{177}Lu-AMS002-1-Fc at day 29.

Meanwhile, the negative control group $^{177}LuCl_3$ showed the same growth curve with the saline group until day 13, then animals started to die due to organ toxicity caused by $^{177}LuCl_3$. ^{177}Lu-AMS002-1-Fc exhibited the most prominent tumor growth delay in contrast to saline group and $^{177}LuCl_3$ group. Neither rapid body weight loss (Fig. 8B) nor other adverse effects, including diarrhea and loss of fur were observed in any group, except the negative control group $^{177}LuCl_3$ until day 13, indicating the safety of ^{177}Lu-AMS002-1-Fc treatment. The sharp decline of the body weight curve in the $^{177}LuCl_3$ group from day 13–15 is because of the death of some mice and all mice died on day 16.

Discussion

Nuclear medicine imaging has been proven invaluable in accelerating theranostics of cancer and precision medicine. Among biological molecules, the nanobody is the smallest biological unit known to bind the target antigen with

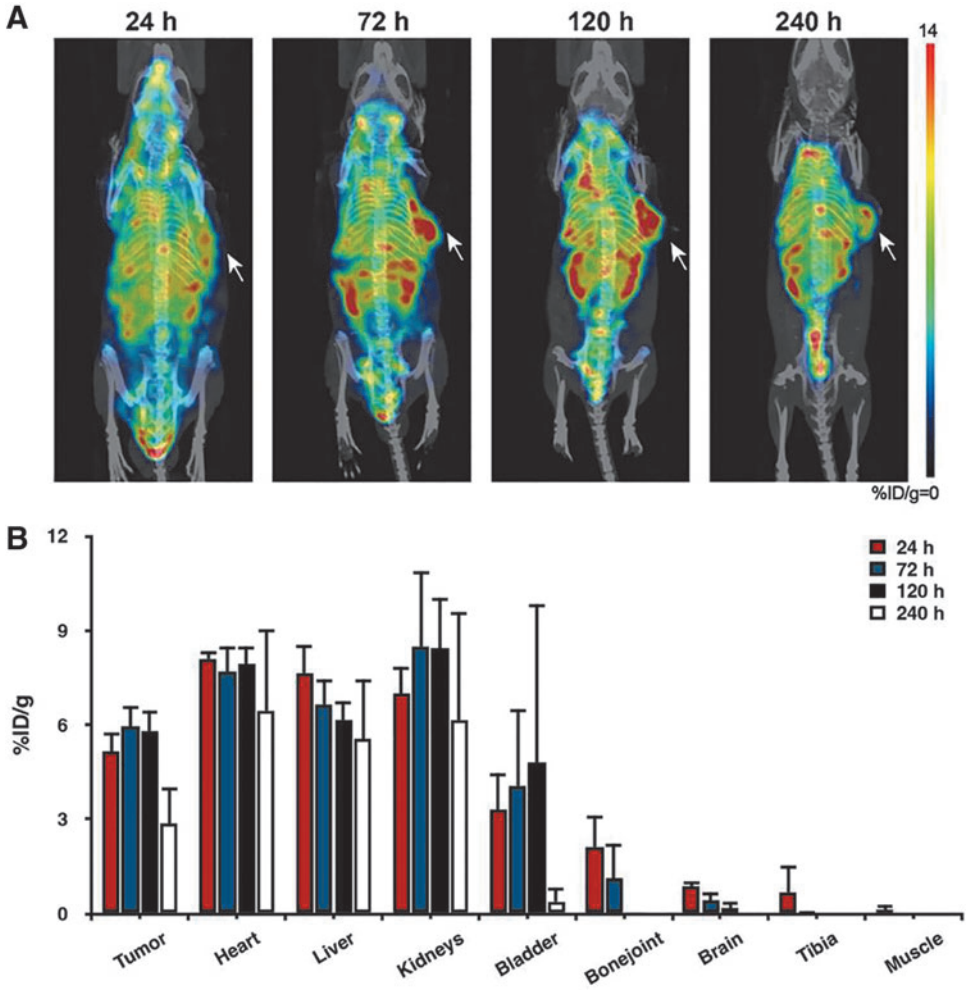

FIG. 7. Micro-SPECT/CT of ^{177}Lu-AMS002-1-Fc-treated HT1080 tumor xenografts. **(A)** Whole-body micro-SPECT/CT imaging and **(B)** semiquantitative analysis of ROIs of BALB/c nude mice bearing HT1080 xenografts (*white arrows*) after injection of 14.8 MBq (140 μg) of ^{177}Lu-AMS002-1-Fc. Each data point represents mean ± SD ($n = 4$).

Downloaded by Nanjing University of Chinese Medicine from www.liebertpub.com at 12/20/23. For personal use only.

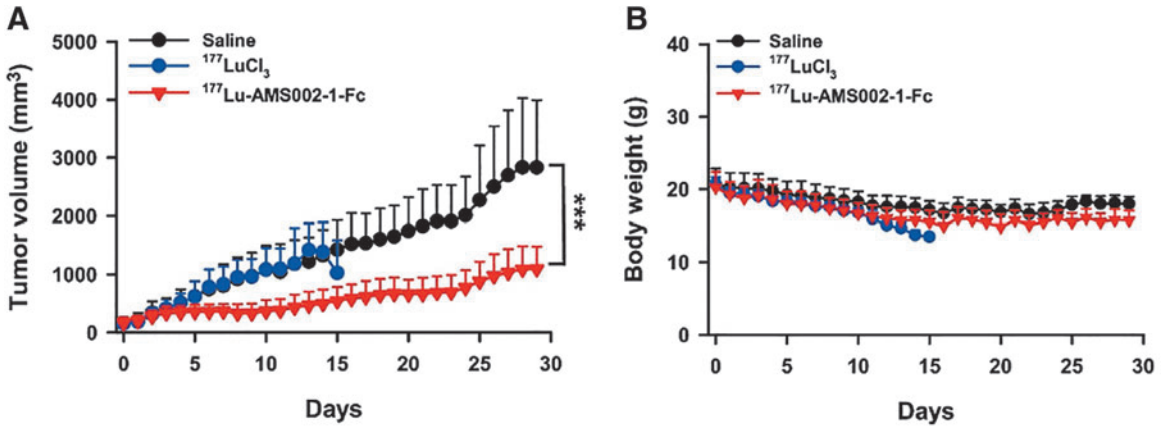

FIG. 8. Analysis of ^{177}Lu-AMS002-1-Fc-treated HT1080 tumor xenografts. **(A)** Tumor growth curves and **(B)** body weight in mice bearing FAPα-positive HT1080 xenografts: Tumor-bearing mice were treated intravenously with 14.8 MBq (140 μg) ^{177}Lu-AMS002-1-Fc, saline, or 14.8 MBq $^{177}LuCl_3$. Each data point represents mean ± SD ($n = 8$–12). ***$p < 0.001$.

Downloaded by Nanjing University of Chinese Medicine from www.liebertpub.com at 12/20/23. For personal use only.

beneficial characteristics of traditional antibodies and small-molecule drugs, including peptides.[29] Nanobodies hold great potential to be employed as diagnostic and therapeutic agents, and radiolabeled nanobodies have become a significant topic related to cancer theranostics.[30,31] However, the lack of an Fc portion has made nanobodies less attractive as imaging/therapeutic regents due to their pharmacokinetic property of a short biological half-life.[32,33]

In this study, two anti-FAPα rAbs were constructed by screening VHHs with high affinity, then fusing IgG4 Fc to prolong the serum half-life and maintain tissue penetration. To the best of our knowledge, this is the first kind of study conducted on FAPα-targeted theranostic radiopharmaceuticals constructed based on nanobody technology.

First, the *in vitro* study showed that the affinity of AMS002-1-Fc with K_D value of 0.547 nM was slightly lower compared with AMS002-2-Fc with K_D value of 0.307 nM. Interestingly, according to the *in vivo* screening study conducted by PET/CT imaging, ^{89}Zr-AMS002-1-Fc exhibits strong tumor uptake and tumor retention ability as well as better biodistribution than ^{89}Zr-AMS002-2-Fc.

In addition, the *ex vivo* biodistribution data are basically consistent with the *in vivo* ROI analysis, except a slight difference between the uptake values of heart and spleen probably due to the drawing ROI of heterogeneous nature of two organs on PET imaging display. The *ex vivo* biodistribution data demonstrated that ^{89}Zr-AMS002-1-Fc had a high tumor-to-muscle ratio (13.18 ± 6.63 at 216 h p.i.). Consequently, AMS002-1-Fc was screened out to conduct the efficacy and safety studies. The results showed that ^{177}Lu-AMS002-1-Fc exhibited excellent radiotherapeutic results.

To construct an effective antibody-based nuclear imaging agent, a fundamental principle is to match the physical half-life of the radioisotope with the pharmacokinetic half-life of the targeting vector.[34,35] According to literature, small-molecule FAPI-04/FAPI-47 have short biological half-life, which is good for diagnostic use, but limit their radiation therapy applications.[36] Recent study has found that ^{177}Lu-FAP-2286, as a peptide-targeted radionuclide therapy agent, shows a little longer retention compared with small molecules.[37] On the other hand, biological molecule ^{131}I-F19 shows slow blood clearance with no internalization that limits their function for efficient diagnosis or therapy of cancer.

The pharmacokinetics study showed that ^{89}Zr-AMS002-1-Fc could be maintained in blood with a half-life of 128 h. Therefore, the biological half-life of the targeted molecule AMS002-1-Fc matches the radionuclide half-life of ^{89}Zr ($t_{1/2} = 78.6$ h) for diagnostic imaging purpose and of ^{177}Lu ($t_{1/2} = 159.6$ h), which is particularly suitable for radiotherapy.

This systemic study demonstrated that ^{89}Zr-AMS002-1-Fc could selectively bind to FAPα-positive cells *in vitro* and accumulate at FAPα-expressing HT1080 tumor *in vivo*. In the SPECT/CT imaging study, the tumor retention of ^{177}Lu-AMS002-1-Fc was sustainable for a long period of time with tumor uptake 5.96% ± 0.64% ID/g at 72 h p.i. and 5.83% ± 0.61% ID/g at 120 h p.i. The above tumor uptake value correlated well with the corresponding radiation therapeutic efficacy study. After 1 week of treatment, the result of radiotherapy efficacy of the ^{177}Lu-AMS002-1-Fc group showed statistically significant difference from negative control groups ($^{177}LuCl_3$ and saline, Fig. 7A), which indicates that ^{177}Lu-AMS002-1-Fc holds potential for radiotherapy of FAPα-expression tumor in patients.

However, due to a limited amount of primary nanobody, the major limitation of the therapeutic study is the absence of the unlabeled AMS002-1-Fc as a control, which does not exclude the therapeutic effect of nanobody itself. Since it is a newly constructed antibody, which has not been expressed with a large amount in the early screening experiment, it is too expensive to express enough nonrelevant nanobodies to conduct a systematic efficacy test. In addition, further studies in larger animals (rats or pet dogs with cancer such as osteosarcoma) would be considered for future studies.

Finally, the experimental results have demonstrated a unique theranostic strategy and a novel radiolabeled rAb against FAPα-expressing tumors. In this study, the radiolabeled nanobody conjugates can specifically deliver radionuclides to tumor tissue with high sensitivity, resulting in high resolution for diagnostic imaging and enough accumulated dosimetry for cancer radiotherapy. A further study

may focus on modification of Fc fragment of AMS002-1-Fc in anticipation of generating new nanobody construct(s) with improved metabolism properties for improved tumor targeting as well.

Conclusion

Altogether, the authors have successfully developed a novel anti-FAPα rAb AMS002-1-Fc with unique tumor-targeting properties *in vivo*. ^{89}Zr/^{177}Lu-AMS002-1-Fc showed good binding affinity, favorable pharmacokinetics, relatively high tumor accumulation, and long tumor retention. These properties warrant further investigation of ^{89}Zr/^{177}Lu-AMS002-1-Fc for moving the improved construct to clinical studies.

Acknowledgments

We gratefully thank the National Natural Science Foundation of China projects (Grant No 11975123) and Jiangsu Planned Projects for Postdoctoral Research Funds (Grant No 2021K078A) for kindly providing financial support. We also thank Yanjun Liu for providing excellent technical assistance.

Authors' Contributions

X.B.T. and Z.W. conceived the idea of the project. J.F.X. wrote the article in addition to designing, performing, and analyzing all experiments. J.F.X., S.H.L., S.S.X., and F.C. performed the experiments. J.F.X., J.D., and J.J.C. collected the information on animals. Z.G.L. and C.R.G. assisted with data analysis. Z.G.L., C.R.G., S.H.L., Z.W., and X.B.T. designed, supervised, and analyzed all experiments, in addition to assisting with article preparation. All authors read and approved the final article.

Ethics Approval

All animal studies were performed in accordance with the protocols provided in the Guide for the Care and Use of Medical Laboratory Animals (Ministry of Health, China).

Disclosure Statement

No competing financial interests exist.

Funding Information

This work was financially supported by the National Natural Science Foundation of China projects (Grant No 11975123) and Jiangsu Planned Projects for Postdoctoral Research Funds (Grant No 2021K078A).

Supplementary Material

Supplementary Figure S1
Supplementary Figure S2
Supplementary Figure S3
Supplementary Figure S4
Supplementary Figure S5
Supplementary Figure S6
Supplementary Table S1

References

1. Scanlan MJ, Raj BK, Calvo B, et al. Molecular cloning of fibroblast activation protein alpha, a member of the serine protease family selectively expressed in stromal fibroblasts of epithelial cancers. Proc Natl Acad Sci USA 1994;91: 5657.
2. Kratochwil C, Flechsig P, Lindner T, et al. (68)Ga-FAPI PET/CT: Tracer uptake in 28 different kinds of cancer. J Nucl Med 2019;60:801.
3. Kalluri R. The biology and function of fibroblasts in cancer. Nat Rev Cancer 2016;16:582.
4. Fischer E, Chaitanya K, Wuest T, et al. Radioimmunotherapy of fibroblast activation protein positive tumors by rapidly internalizing antibodies. Clin Cancer Res 2012; 18:6208.
5. Baum RP, Schuchardt C, Singh A, et al. Feasibility, Biodistribution and Preliminary Dosimetry in Peptide-Targeted Radionuclide Therapy (PTRT) of Diverse Adenocarcinomas using (177)Lu-FAP-2286: First-in-Human Results. J Nucl Med 2022;63:415.
6. Liu F, Qi L, Liu B, et al. Fibroblast activation protein overexpression and clinical implications in solid tumors: A meta-analysis. PLoS One 2015;10:e0116683.
7. Welt S, Divgi CR, Scott AM, et al. Antibody targeting in metastatic colon cancer: A phase I study of monoclonal antibody F19 against a cell-surface protein of reactive tumor stromal fibroblasts. J Clin Oncol 1994;12:1193.
8. Assadi M, Rekabpour SJ, Jafari E, et al. Feasibility and therapeutic potential of 177Lu-fibroblast activation protein inhibitor-46 for patients with relapsed or refractory cancers: A Preliminary Study. Clin Nucl Med 2021;46:e523.
9. Ferdinandus J, Fragoso Costa P, Kessler L, et al. Initial clinical experience with (90)Y-FAPI-46 radioligand therapy for advanced stage solid tumors: A case series of nine patients. J Nucl Med 2022:jnumed.121.262468.
10. Kuyumcu S, Kovan B, Sanli Y, et al. Safety of Fibroblast Activation Protein-Targeted Radionuclide Therapy by a Low-Dose Dosimetric Approach Using 177Lu-FAPI04. Clin Nucl Med 2021;46:641.
11. LeBeau AM, Brennen WN, Aggarwal S, Denmeade SR. Targeting the cancer stroma with a fibroblast activation protein-activated promelittin protoxin. Mol Cancer Ther 2009;8:1378.
12. Ryabtsova O, Jansen K, Van Goethem S, et al. Acylated Gly-(2-cyano)pyrrolidines as inhibitors of fibroblast activation protein (FAP) and the issue of FAP/prolyl oligopeptidase (PREP)-selectivity. Bioorg Med Chem Lett 2012; 22:3412.
13. Ma H, Li F, Shen G, et al. Synthesis and preliminary evaluation of (131)I-labeled FAPI tracers for cancer theranostics. Mol Pharm 2021;18:4179.
14. Xu M, Zhang P, Ding J, Chen J, Huo L, Liu Z. Albumin binder-conjugated fibroblast activation protein inhibitor radiopharmaceuticals for cancer therapy. J Nucl Med 2022: jnumed.121.262533.
15. Tsai TY, Yeh TK, Chen X, et al. Substituted 4-carboxymethylpyroglutamic acid diamides as potent and selective inhibitors of fibroblast activation protein. J Med Chem 2010;53:6572.
16. Jansen K, Heirbaut L, Verkerk R, et al. Extended structure-activity relationship and pharmacokinetic investigation of (4-quinolinoyl)glycyl-2-cyanopyrrolidine inhibitors of fibroblast activation protein (FAP). J Med Chem 2014;57: 3053.

Downloaded by Nanjing University of Chinese Medicine from www.liebertpub.com at 12/20/23. For personal use only.

17. Hofheinz RD, al-Batran SE, Hartmann F, et al. Stromal antigen targeting by a humanised monoclonal antibody: An early phase II trial of sibrotuzumab in patients with metastatic colorectal cancer. Onkologie 2003;26:44.
18. Scott AM, Wiseman G, Welt S, et al. A Phase I dose-escalation study of sibrotuzumab in patients with advanced or metastatic fibroblast activation protein-positive cancer. Clin Cancer Res 2003;9:1639.
19. Brennen WN, DL JT, Jiang W, et al. Overcoming stromal barriers to immuno-oncological responses via fibroblast activation protein-targeted therapy. Immunotherapy 2021;13:155.
20. Thurber GM, Schmidt MM, Wittrup KD. Factors determining antibody distribution in tumors. Trends Pharmacol Sci 2008;29:57.
21. Wu AM. Engineered antibodies for molecular imaging of cancer. Methods 2014;65:139.
22. Liu M, Li L, Jin D, Liu Y. Nanobody-A versatile tool for cancer diagnosis and therapeutics. Wiley Interdiscip Rev Nanomed Nanobiotechnol 2021;13:e1697.
23. Chakravarty R, Goel S, Cai W. Nanobody: The ''magic bullet'' for molecular imaging? Theranostics 2014;4:386.
24. Mir MA, Mehraj U, Sheikh BA, Hamdani SS. Nanobodies: The ''Magic Bullets'' in therapeutics, drug delivery and diagnostics. Hum Antibodies 2020;28:29.
25. Li D, Cheng S, Zou S, et al. Immuno-PET Imaging of (89)Zr labeled Anti-PD-L1 domain antibody. Mol Pharm 2018;15:1674.
26. Banerjee SR, Kumar V, Lisok A, et al. (177)Lu-labeled low-molecular-weight agents for PSMA-targeted radiopharmaceutical therapy. Eur J Nucl Med Mol Imaging 2019;46:2545.
27. Ruigrok EAM, van Vliet N, Dalm SU, et al. Extensive preclinical evaluation of lutetium-177-labeled PSMA-specific tracers for prostate cancer radionuclide therapy. Eur J Nucl Med Mol Imaging 2021;48:1339.
28. Lakes AL, An DD, Gauny SS, et al. Evaluating (225)Ac and (177)Lu radioimmunoconjugates against antibody-drug conjugates for small-cell lung cancer. Mol Pharm 2020;17:4270.
29. Bathula NV, Bommadevara H, Hayes JM. Nanobodies: The future of antibody-based immune therapeutics. Cancer Biother Radiopharm 2021;36:109.
30. Weber WA, Czernin J, Anderson CJ, et al. The future of nuclear medicine, molecular imaging, and theranostics. J Nucl Med 2020;61(Suppl 2):263S.
31. Lecocq Q, De Vlaeminck Y, Hanssens H, et al. Theranostics in immuno-oncology using nanobody derivatives. Theranostics 2019;9:7772.
32. Verhaar ER, Woodham AW, Ploegh HL. Nanobodies in cancer. Semin Immunol 2020;52:101425.
33. Bell A, Wang ZJ, Arbabi-Ghahroudi M, et al. Differential tumor-targeting abilities of three single-domain antibody formats. Cancer Lett 2010;289:81.
34. Deri MA, Zeglis BM, Francesconi LC, Lewis JS. PET imaging with (8)(9)Zr: From radiochemistry to the clinic. Nucl Med Biol 2013;40:3.
35. Dash A, Chakraborty S, Pillai MR, Knapp FF, Jr. Peptide receptor radionuclide therapy: An overview. Cancer Biother Radiopharm 2015;30:47.
36. Lindner T, Loktev A, Altmann A, et al. Development of quinoline-based theranostic ligands for the targeting of fibroblast activation protein. J Nucl Med 2018;59:1415.
37. Zboralski D, Osterkamp F, Simmons AD, et al. Preclinical evaluation of FAP-2286, a peptide-targeted radionuclide therapy (PTRT) to fibroblast activation protein alpha (FAP). Ann Oncol 2020;31:S488.

Downloaded by Nanjing University of Chinese Medicine from www.liebertpub.com at 12/20/23. For personal use only.